Biophysical Journal, Volume 98

Supporting Material

Tertiary and Secondary Structure Elasticity of a Six-Ig Titin Chain

Eric H. Lee, Jen Hsin, Eleonore von Castelmur, Olga Mayans, and Klaus Schulten

Supporting Material

Movies

Movie S1. (IG6-extend-only.mpg) This movie shows the trajectory generated from simulation *simEXT* where Ig6 was extended (straightened) without unfolding any of the domains. The force-extension curve from the simulation is also displayed, a red marker indicating the extension reached in the trajectory. The marker does not advance with constant speed, reflecting the fact that even as Ig6 is just being straightened out in its regime of tertiary structure elasticity, interactions due to the interdomain arrangements of the Ig-pairs give rise to significant energy barriers

Movie S2. (IG6-noDS-wide.mpg) This movie shows the trajectory generated from simulation *simSTR1* where Ig6 was extended until completely unfolded. The pattern of sequential Ig-domain rupturing produces a force-extension profile similar to that seen in AFM experiments stretching engineered titin Ig-domain polyproteins.

Movie S3. (IG6-noDS-zoom.mpg) This movie shows the trajectory generated from simulation *simSTR1* where Ig6 was extended until completely unfolded. This movie differs from Movie S2 in that it pauses and zooms onto the particular Ig-domain being ruptured during forced extension. One can recognize that the rupturing of one domain leads to relaxation of other domains. For example, when domain I69 (purple) is just beginning to unravel, domain I66 (blue) actually ruptures first, and I69 relaxes its terminal β-strands, refolding them back into a β-sheet.

Movie S4. (IG6-DS-wide.mpg) This movie shows the trajectory from simulation *simSTR2* where the sidechains of cysteines that are spatially adjacent to each other were disulfide-bonded. In this case, I65, 66, 67, and 69 exhibit disulfide bonds, while I68 and 70's do not. The disulfide bonds inhibit the respective Ig-domains from complete unraveling, but do not have an effect on the order of domain rupture. Indeed, the sequence of Ig-domain ruptures seen in Movie S4 is the same as that in Movies S2 and S3 (i.e., the domains rupture in the order I65 $\rightarrow$ I70 $\rightarrow$ I66 $\rightarrow$ I67 $\rightarrow$ I69 $\rightarrow$ I68), with the peripheral domains rupturing before the central domains.

Movie S5. (IG6-DS-zoom.mpg) This movie shows the trajectory from simulation *simSTR2* where the sidechains of cysteines spatially adjacent to each other have been disulfide-bonded as in Movie S4. The movie zooms onto the particular domain that is being unraveled during forced extension.

Simulation Methods

Equilibrium and ABF simulations. Atomic coordinates of titin Ig-domains I65-70 were taken from the crystal structure (PDB entry code 3B43) (1). The Ig6 structure contains six Ig-domains connected in series. The simulation topology of the protein and missing hydrogen atoms were generated using psfgen (2) with the CHARMM27 topology file (3). All simulation systems were solvated using the VMD (4) plugin Solvate in a periodic box of explicit water, large enough to accommodate the protein and the space required for stretching Ig6 out completely. The long axis of the protein was aligned along the y-axis of the water box. Neutralizing counter ions were added using the VMD plugin Autoionize to reach an ionic concentration of 150 mM NaCl. Acidic and basic residues such as Asp, Glu, Lys, and Arg were modeled in their charged form. The protonation state of His residues was chosen to favor hydrogen bonding where possible. Disulfide bonds in the case of simulations *simEQ-str2* and *simSTR2*, defined in Table 1, were modeled for cysteine pairs CYS23:CYS74 (I65), CYS119:CYS170 (I66), CYS215:CYS277 (I67), and CYS402:CYS464 (I69).

All free-dynamics equilibrium simulations were carried out following energy minimization for 10,000 conjugate gradient steps. The equilibrated Ig6 structure from *simEQ* was re-solvated in an enlarged water box for *simEQ-ext*. The final extended structure from *simEXT* was used as the starting structure for *simEQ-str1* and *simEQ-str2* and re-solvated in a further enlarged water box to accommodate the subsequent SMD simulations. In *simEQ-ext*, *simEQ-str1*, and *simEQ-str2*, Ig6 was aligned in the water box such that it would stretch along the long axis of the water box in the subsequent SMD stretching simulations. Equilibrations of the individual connected Ig-domain pairs from Ig6 were performed in *simEQ-ab*, *simEQ-bc*, *simEQ-cd*, *simEQ-de*, *simEQ-ef* for I65-66, I66-67, I67-68, I68-69, and I69-70, respectively. The root mean squared deviation (RMSD) for the backbone carbon atoms served as a criterion for determining whether the systems were fully equilibrated.

Equilibrium and adaptive biasing force (ABF) simulations were performed using a multiple time-stepping algorithm (5; 6) which computed covalent bonds every time step, short-range non-bonded interactions every second timestep, and long range electrostatic forces every fourth timestep (1-2-4 stepping). For SMD simulations, 1-1-1 stepping was employed in order to minimize energy drift (7). Equilibrium and SMD simulations employed an inte-

gration timestep of 1 fs, while ABF simulations employed 2 fs.

For ABF simulations, a restraining harmonic potential was applied to constrain the motion along the reaction coordinate into either a bending-only or twisting-only motion. In the case of a bending motion, the restraining potential permitted extension only along the XY plane containing the N- and C-termini and the interdomain linker region. In the case of a twisting motion, the restraining potential permitted extension only along the normal to the XY plane defined by the N- and C-termini and interdomain linker region. Every ABF simulation reported here is a composite of multiple simulation runs, each sampling approximately ten degrees of bending or twisting rotation. For example, in *simAB-b* fifty degrees of bending angle rotation were covered by five individual simulations. The size for each ABF sampling bin in the simulations was 0.1 Å. All ABF simulations were performed long enough to observe convergence (even distribution of sampling across the reaction coordinate) of the system for accurate description of the potential of mean force.

Simulated system geometry and size. The system used to equilibrate Ig6 initially (in *simEQ*) consisted of titin Ig6 (8,375 atoms), 71,482 water molecules, and Na^+/Cl^- ions, for a total system size of 223,594 atoms in a periodic box of dimension $110 \times 339 \times 63$ Å^3. The system which accommodates the elongation of Ig6 into a straight chain (*simEQ-ext*) consisted of titin Ig6, 89,244 water molecules, and Na^+/Cl^- ions, for a total system size of 276,978 atoms in a periodic box of dimension $114 \times 353 \times 72$ Å^3. The system which accommodates the full unfolding of Ig6 without disulfide bond restraints (*simEQ-str1*) consisted of titin Ig6, 208,491 water molecules, and Na^+/Cl^- ions, for a total system size of 635,409 atoms in a periodic box of dimension $2045 \times 60 \times 53$ Å^3. The system which accommodated the full unfolding of Ig6 with disulfide bond restraints (*simEQ-str2*) consisted of titin Ig6, 138,347 water molecules, and Na^+/Cl^- ions, for a total system size of 424,567 atoms in a periodic box of dimension $1197 \times 64 \times 58$ Å^3. This box was smaller than that used for *simEQ-str1* since the disulfide bonds prevent this restrained Ig6 from fully unraveling.

Five further systems simulated involved the individual Ig-pairs from Ig6: I65-I66, I66-67, I67-68, I68-69, and I69-70. The system for I65-66 included 24,801 water molecules, and ions for a total system size of 77,512 atoms in a periodic box of dimension $131 \times 82 \times 77$ Å^3; the system for I66-67 included 23,045 water molecules, and ions for a total system size of 72,165 atoms in a periodic box of dimension $138 \times 71 \times 77$ Å^3; the system for I67-68 included 23,175 water molecules, and ions for a total system size of 72.575 atoms in a periodic box of dimension $136 \times 74 \times 77$ Å^3. The system for I68-69 included 23,015 water molecules, and ions for a total system size of 72,126 atoms in a periodic box of dimension $129 \times 81 \times 74$ Å^3; the system for I69-70 included 24,706 water molecules, and ions for a total system size

of 77,182 atoms in a periodic box of dimension 131 × 83 × 75 Å^3.

Summary of simulations. The simulations carried out in this study are listed in Table 1. *simEQ*, *simEQ-ext*, *simEQ-str1*, and *simEQ-str2* were equilibrium simulations of Ig6 in water boxes of various sizes to accommodate SMD simulations. *simEQ-ab*, *simEQ-bc*, *simEQ-cd*, *simEQ-de*, and *simEQ-ef* were equilibrium simulations of each Ig-pair in Ig6, corresponding to I65-66, I66-67, I67-68, I68-69, and I69-70, respectively. *simAB-b*, *simBC-b*, *simCD-b*, *simDE-b*, *simEF-b* were ABF simulations sampling a hinge type motion, whereas *simAB-t*, *simBC-t*, *simCD-t*, *simDE-t*, *simEF-t* were ABF simulations sampling a torsional motion for each Ig-pair. In *simEXT*, SMD was performed to extend Ig6 without unfolding any of the domains. In *simSTR1* and *simSTR2*, the entire Ig6 ensemble was stretched and unfolded via SMD, with disulfide bonds enforced in the latter. All simulations were performed at the National Center for Supercomputing Applications (NCSA) at the University of Illinois at Urbana-Champaign.

Analysis of simulations. System coordinates were saved every picosecond, and analysis was performed using the time-line plugin of the program VMD (4). Structural changes in the calculated models were monitored by calculating the root mean squared deviation (RMSD) of their backbone atoms. The end-to-end distance profile of a stretched system is based on the distance between the two stretched or between stretched and fixed terminal C_α atoms. The change of the end-to-end distance is defined as the extension of the system. The hinge and torsion angles were derived from the geometric relationship between the separation of the tips of the Ig-domains along the ABF reaction coordinate and the position of these tips along their restricted arcs of motion.

Modeling of Tertiary Structure Elasticity in a Multidomain Chain

Derivation of multidomain chain extension under force Here we derive the average overall end-to-end distance of the chain, $\langle X \rangle$, when a force f is applied. We start from the average length of a linker pair j given by

$$\langle x_j \rangle_{\tilde{V}_j} \;=\; \int_{-\infty}^{+\infty} x_j \hat{p}_j(x_j) dx_j \;=\; \int_{-\infty}^{+\infty} x_j \exp[-\hat{V}_j(x_j)/k_BT] dx_j / \int_{-\infty}^{+\infty} \exp[-\hat{V}_j(x_j)/k_BT] dx_j. \tag{1}$$

The integral in the numerator can be expressed, using $\hat{V}_j(x_j) \;=\; V_j(x_j) - f x_j$,

$$\int_{-\infty}^{+\infty} x_j \exp[-\hat{V}_j(x_j)/k_BT] dx_j \;=\; Z_j \langle x_j \exp[f x_j/k_BT] \rangle_{V_j}, \tag{2}$$

where Z_j is defined in the text and where we define the average $\langle f(x)\rangle_{V_j} = \int_{-\infty}^{+\infty} f(x)\exp[-V_j(x_j)/k_BT]dx_j$. One can similarly rewrite the integral in the denominator of Eq. 1, which leads to

$$\langle x_j\rangle_{\hat{V}_j} = \langle x_j \exp[fx_j/k_BT]\rangle_{V_j}/\langle\exp[fx_j/k_BT]\rangle_{V_j}. \quad (3)$$

The average overall end-to-end distance, $\langle X\rangle = \sum_{j=1}^{N}\langle x_j\rangle_{\hat{V}_j}$, can then be written

$$\langle X\rangle = \sum_{j=1}^{N}\left[\langle x_j \exp[fx_j/k_BT]\rangle_{V_j}/\langle\exp[fx_j/k_BT]\rangle_{V_j}\right] \equiv g(f). \quad (4)$$

Tertiary structure elasticity arising from the hinge bending motions. In Figure S1A, the length distribution of each Ig6 linker pair (open circles in Figure S1A) was fitted to a sum of two Gaussian functions (Eq. 5; solid lines in Figure S1A). Two conditions are imposed on the fitting parameters: (1) $c1$ and $c2$ need to be greater than zero to ensure each term of Eq. 5 is Gaussian, so that the Fourier transform in Eq. 4 is numerically feasible and straightforward; (2) $b1$ and $b2$ need to be within the range of attainable length of an Ig linker pair, since $b1$ and $b2$ represent the most probable lengths of the linker. Additionally, the fitting expressions need to vanish outside of the range of feasible Ig6 domain pair extension ($x_{j,min} \leq x_j \leq x_{j,max}$). The parameters, satisfying these criteria, are listed in Table S1. Calculations of $P(X)$ and the subsequent force-extension response of the multidomain chain employed these parameters.

Table S1: Parameters used in calculations of $P(X)$ and the force-extension response of the multidomain chain. All lengths are shown in units of Å. $x_{j,min}$ and $x_{j,max}$ are estimated from ABF data representing the achievable end-to-end length for domain pair j; $\Delta x_{j,max}$, representing the maximum extension contributed by domain pair j, is estimated via $x_{j,max}$ - $\bar{x}_j$.

domain pair	$a1$	$b1$	$c1$	$a2$	$b2$	$c2$	$x_{j,min}$	$x_{j,max}$	$\Delta x_{j,max}$
AB	0.562	54.327	0.330	0.748	59.702	0.026	52	78	∼19
BC	0.542	58.336	0.015	0.742	74.204	0.076	51	82	∼18
CD	0.720	86.400	0.140	0.370	76.650	0.030	57	88	∼7
DE	0.980	64.810	0.060	1.010	88.110	0.580	62	90	∼19
EF	0.893	85.711	0.109	0.094	75.452	0.010	62	90	∼7

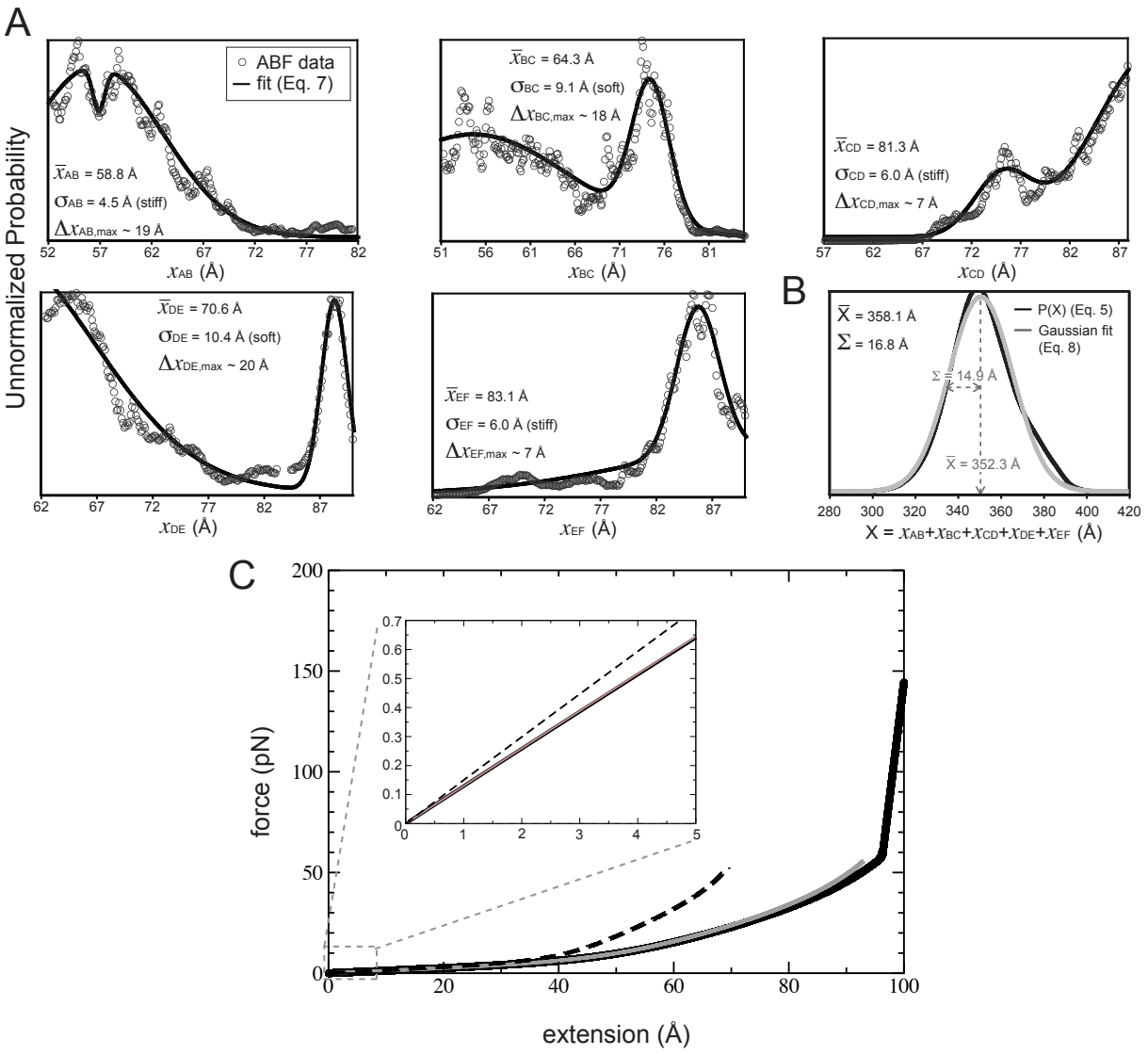

Figure S 1: Tertiary structure elasticity of a multidomain chain. (A) The PMF resulting from ABF simulations can be related to length distribution for an individual Ig linker pair, represented by open circles. Fits $p_j(x_j)$ in the form of Eq. 5 are plotted as solid lines. Also shown in the plots are the mean end-to-end length of each domain pair, $\bar{x}_j$, the root mean square deviation of each $p_j(x_j)$, σ_j, and the approximate maximum extension of each domain pair, $\Delta x_{j,max}$. The hinges are labeled as stiff or soft depending on their σ_j values. (B) The overall length distribution for the chain of five Ig domain pairs, computed using Eq. 4 is shown (black), the Gaussian fit (Eq. 6) being depicted in gray. (C) Shown is the overall extension of the modeled multidomain chain in response to mechanical force. At small forces ($f < 5$ pN), the force-extension curve is linear (inset). The dashed curve is calculated from considering only the bending motion in the multidomain chain; the gray curve includes both bending and twisting motions in the calculation; the black solid curve incorporates also the stretching degree of freedom in each domain.

Tertiary structure elasticity arising from the hinge twisting motions. The chain extension stemming from the bending motion within each domain pair, described in the text in detail, results in approximately 70 Å of overall chain extension (Figure 5C). Further extension arises from other degrees of freedom, one of which being the twisting motions of the domain pairs in the Ig6 chain, also characterized by ABF simulations (Figure 4B).

We described chain extension resulting from twisting motions following the same treatment as applied for bending motions. The potential of mean force for each domain pair, obtained through ABF (Figure 4B), is first translated into a length distribution using Eq. 2, shown as open circles in Figure S2. The length distribution is then fitted using Eq. 5 (black curves in Figure S2). The fitting parameters are listed in Table S2. Note that the maximum extension stemming from the twisting motion, $\Delta X_{twisting} = \sum_{j=1}^{5} \Delta x_{j,max}$, add up to ∼34 Å, and yet, as demonstrated in Figures 3B and S1C, addition of twisting motions only extends the multidomain chain by another 23 Å. This is due to the fact that, realistically, the hinge bending and twisting motions are not complementary, but are coupled. The coupling of bending and twisting is apparent considering that when the softer bending motion is completely exhausted, the Ig6 chain has attained its maximum length, and the further extension at higher forces through twisting actually cannot come into play. The precise nature of the coupling between the bending and twisting degrees of freedom is worthy of further investigation.

Table S2: Fitting parameters used in Figure S2. All lengths are in units of Å.

domain pair	$a1$	$b1$	$c1$	$a2$	$b2$	$c2$	$x_{j,min}$	$x_{j,max}$	$\Delta x_{j,max}$
AB	0.597	65.427	0.837	0.460	64.405	0.293	60	69	∼4
BC	0.612	65.282	0.472	1.179	76.165	0.018	60	90	∼15
CD	0.924	69.941	0.222	0.271	66.490	7.870	65	75	∼5
DE	0.137	71.985	0.928	0.920	74.615	0.329	70	80	∼6
EF	0.955	76.070	0.277	0.053	72.006	0.494	70	80	∼4

Hinge twisting can be combined with hinge bending to describe the overall chain elasticity using Eqs. 5 and 20, with j labeling the five hinge bending and five hinge twisting angles. The red trace in Figure 3B incorporates both bending and twisting motions, but still deviates from the force-extension curve actually seen in the simulation by several Å. The difference stems from reversible stretching of the individual domains as discussed now.

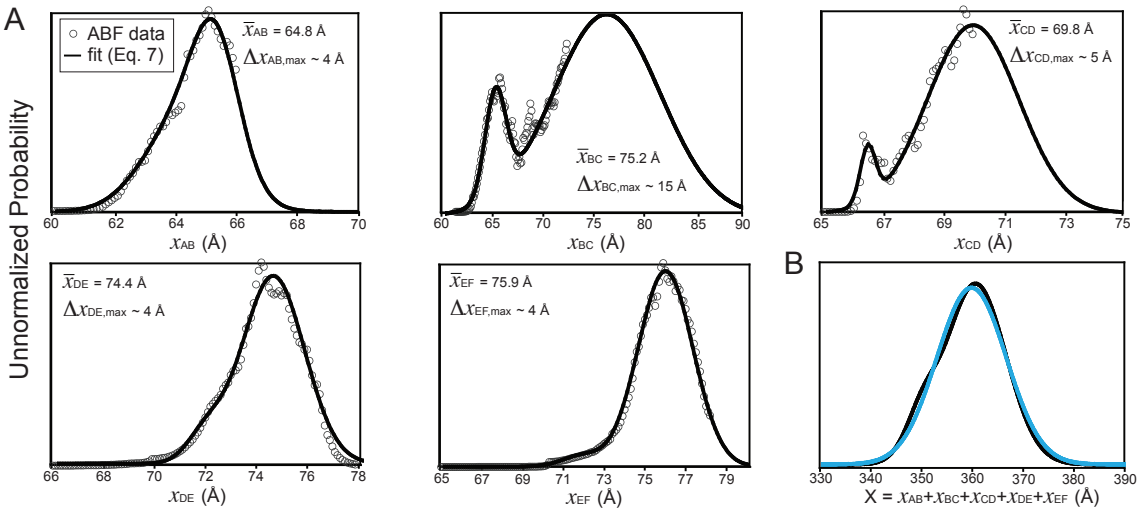

Figure S2: Multidomain chain extension stemming from hinge twisting. Length distribution data computed from ABF simulation are shown as open circles, with the fitting equations (according to Eq. 5) shown as solid curves. For each domain pair, the average end-to-end domain pair length, $\bar{x}_j$, and the estimated maximum extension, $\Delta x_{j,max}$, are also given. Fitting equations were allowed to take values within allowable domain pair extension length $x_j \leq 90$ Å, even if ABF simulations did not sample these regions.

Elasticity arising from the intrinsic stretching of individual Ig domains. In Figure 3B, one recognizes that the multidomain chain model reproduces very well the rise in the force-extension profile of the SMD pulling of the Ig6 chain. However, the predicted Ig6 extension ends at ∼93 Å, while a total extension of ∼100 Å was achieved via simulation. The 93-100 Å extension comes from degrees of freedom other than the bending and twisting motions of the connected domain pairs, namely, from end-to-end stretching of individual domains. To verify this hypothesis, an equilibrium simulation (*sim-EQ-I65*) was carried out with one Ig domain (I65), and its end-to-end extension was measured for each frame of the trajectory (Figure S3A). As can be seen in Figure S3A, the end-to-end extension of an Ig domain fluctuates around 1-2 Å; with six domains in tandem, a ∼10-Å extension indeed arises. Figure S3B shows that the extension is Gaussian distributed, contributing a degree of linear elasticity.

Additional Results

Extension vs. time resulting from simulation *simEXT*. In simulation *simEXT*, Ig6 was pulled by an SMD spring with spring constant k_s. The average extension of Ig6, $\langle x(t) \rangle$,

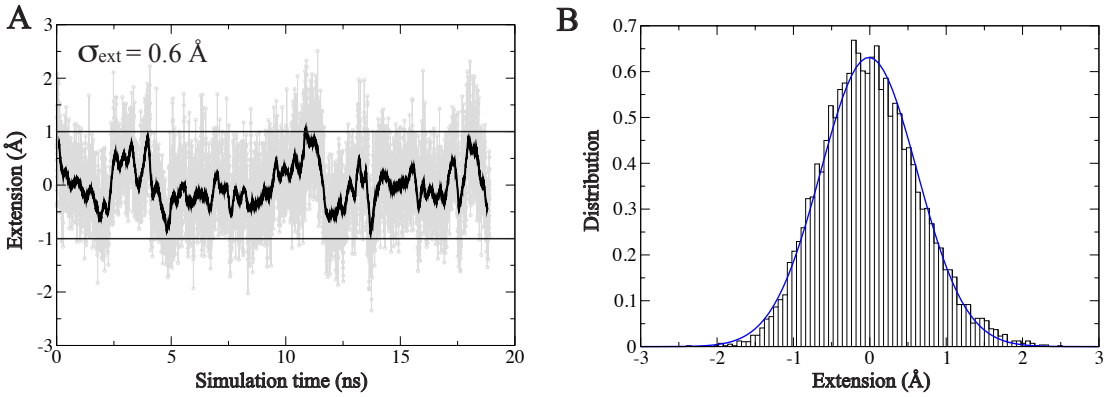

Figure S3: (A) Fluctuation in end-to-end extension of an Ig domain vs. time for *sim-EQ-I65*. Ig domain length extension is defined to be the difference between the end-to-end length at the given frame and the average value (over the simulation); horizontal lines are drawn at +1 and -1 Å extensions as a guide to the eyes. The I65 end-to-end extension fluctuates by 1-2 Å. Such length fluctuation explains the remaining extension (∼10 Å) seen in the SMD simulation of Ig6 not covered by hinge bending and twisting. (B) Distribution of end-to-end extension. This distribution can be well-described by a Gaussian fit (blue), with RMSD value of $\sigma = 0.6$ Å.

is determined by Eq. 16. For $|f_{\rm chain}[x(t)]| \ll |k_s(x - vt)|$ and $\exp(-k_s t/\gamma) \to 0$ (i.e., for $t \gg \gamma/k_s = 20$ ps), the average extension is $\langle x(t)\rangle \sim vt - \Delta x$, where $\Delta x = v\gamma/k_s$ is the extension of the SMD spring. Δx, is estimated to be 0.2 Å (see main text) given the pulling velocity, $v = 10$ Å/ns, the friction coefficient, γ, dictated by a diffusion coefficient $D = 1.5 \times 10^{-6}$ cm^2/s typical for a protein, and the SMD spring constant $k_s = 3k_BT/\mathring{A}^2$ employed in the SMD simulation. In Figure S4 the protein extension as a function of time seen in simulation *simEXT* is plotted as a blue trace and the value of vt is plotted as an orange trace. The difference between protein extension and vt is shown in the inset displaying a zoomed-in region of the plot; one recognizes that the difference between $x(t)$ and vt is indeed about 0.2 Å, as estimated in the text.

Proof of $\partial g(f)/\partial f \geq 0$. We note first the property that holds for any $h(x)$

$$\langle h(x)\rangle_{\tilde{V}} = \langle h(x)\exp(\beta f x)\rangle_V / \langle \exp(\beta f x)\rangle_V \tag{5}$$

where we define as in the main text

$$\tilde{V}(x) = V(x) - f x \tag{6}$$

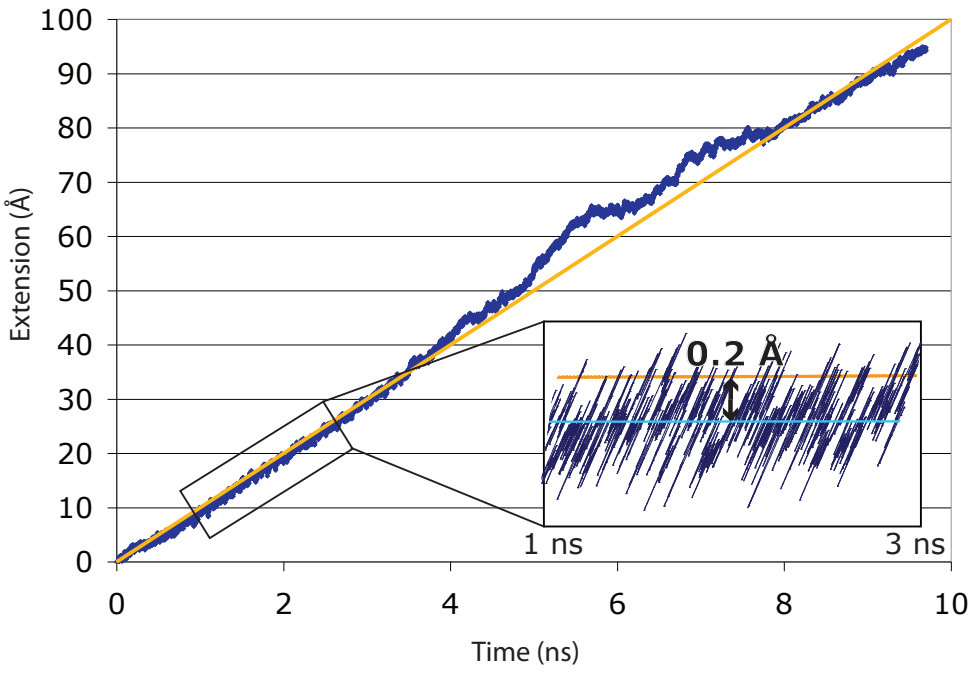

Figure S4: Extension vs. time plot for *simEXT*. The blue trace is the measured extension of Ig6 during the SMD pulling simulation, with pulling velocity 10 Å/ns. The orange line is $x(t) = vt$. The Ig6 extension lags consistently behind the $x(t) = vt$ trace by approximately 0.2 Å, as shown in the inset, which displays the averaged extension by a light blue trace.

and

$$\langle h(x)\rangle_W = \int_{-\infty}^{+\infty} dx\, h(x)\, \exp[-\beta W(x)] / \int_{-\infty}^{+\infty} dx\, \exp[-\beta W(x)] \tag{7}$$

This property can be readily derived and has been used also in the main text.

Defining presently, in analogy to Eq. 11 in the main text,

$$g(f) = \sum_j \left(\langle x_j\, \exp(\beta\, f\, x_j)\rangle_V \,/\, \langle \exp(\beta\, f\, x_j)\rangle_V\right) \tag{8}$$

one obtains, taking the derivative,

$$\frac{\partial g(f)}{\partial f} = \beta \sum_j \left[\frac{\langle x_j^2\, \exp(\beta\, f\, x_j)\rangle_V}{\langle \exp(\beta\, f\, x_j)\rangle_V} - \left(\frac{\langle x_j\, \exp(\beta\, f\, x_j)\rangle_V}{\langle \exp(\beta\, f\, x_j)\rangle_V}\right)^2\right] \tag{9}$$

Employing Eq. (5), this can be written

$$\frac{\partial g(f)}{\partial f} \;=\; \beta \sum_j \langle \big(x_j^2 \;-\; \langle x_j \rangle_{\tilde{V}}^2 \big) \rangle_{\tilde{V}} \tag{10}$$

This expression can be expressed

$$\frac{\partial g(f)}{\partial f} \;=\; \beta \sum_j \langle (x_j \;-\; \langle x_j \rangle_{\tilde{V}})^2 \rangle_{\tilde{V}} \tag{11}$$

Since all contributions in the sum are positive we can conclude $\partial g(f)/\partial f \;\geq\; 0$.

We like to note, finally, that Eq. (8) can be stated in the form

$$g(f) \;=\; k_{\rm B}T \, \frac{\partial}{\partial f} \sum_j \log \langle \exp(\beta \, f \, x_j) \rangle_V \tag{12}$$

The sum on the right hand side of this equation can be recognized as the negative free energy difference $\Delta F(f) \;=\; F(f) \,-\, F(0)$ of the uncoupled particles with coordinates x_j, all subjected to the same force f. Accordingly, we obtain

$$g(f) \;=\; -\, k_{\rm B}T \, \frac{\partial \Delta F(f)}{\partial f} \; . \tag{13}$$

Secondary structure elasticity of titin I65-70 simulated with disulfide bonds. In *simSTR1* it was observed that the sequence of one-by-one domain rupture is related to position of the domains along the Ig6 chain: the outside domains rupture before the inside ones. One structural feature of titin Ig-domains is the presence of cysteine residues which can form internal disulfide bonds across the β-sheets of Ig-domains and may serve to stabilize the titin chain under oxidizing conditions (8). In *simSTR1*, cysteine-cysteine disulfide bonds were not modeled into any of the Ig-domains in order to permit full extension of all six domains. To address how intra-domain disulfide bonds alter the overall Ig6 extension, we modeled disulfide bonds across naturally neighboring cysteines in I65, I66 I67, and I69. The cysteines in I68 and I70 were too far apart to warrant a disulfide bond within those domains. The new Ig6 construct, therefore, contained four Ig-domains with a single disulfide bond, and two Ig-domains without such bonds.

After equilibrating the Ig6-disulfide construct in *simEQ-str2*, the N-terminal α-carbon of I65 was fixed in place and a force applied to the C-terminal α-carbon of I70 in *simSTR2* to stretch and unfold Ig6. The force-extension curve for this simulation is shown in Figure S6A,

which shows the expected shorter overall extension. The secondary structure downstream and upstream of the cysteines involved was free to rupture, but β-strands in between are effectively protected by the additional bond. The force peaks labeled in Figure S6A as (*ii*) to (*vii*) correspond to the rupture of individual Ig-domains; peak (*ii*) corresponds to the rupture of I65, (*iii*) to I70, *iv* to I66, (*v*) to I67, (*vi*) to I69, and (*vii*) to I68, shown in Figure S6B. The sequence of rupture, surprisingly, is identical to that observed in *simSTR1* which did not have modeled disulfide bonds, i.e., outside domains rupture before inside ones for Ig6 with and without disulfide bonds. The order of domain rupture in both cases coincided with the rupture of terminal Ig-domains (i.e. I65 and I70) of the chain before the internal domains, suggesting strongly that the increased compliance and flexibility of terminal domains, which are only joined to an adjacent Ig-domain on one end and allowed to freely fluctuate to the applied force at the other end, permit the terminal β-strands of those domains to align perpendicularly with the applied force such that rupture occurs through the sequential rupture of individual hydrogen bonds rather than a directed shearing motion against multiple hydrogen bonds lengthwise along the β-strand.

Naturally, I65, I66, I67, and I69 did not unravel completely because of their disulfide bonds. The unfolding trajectory for *simSTR2* is shown in movies S4 and S5 which include a force-extension trace illustrating the correlation of each labeled force peak in the force-extension curve to the rupture of an individual Ig-domain.

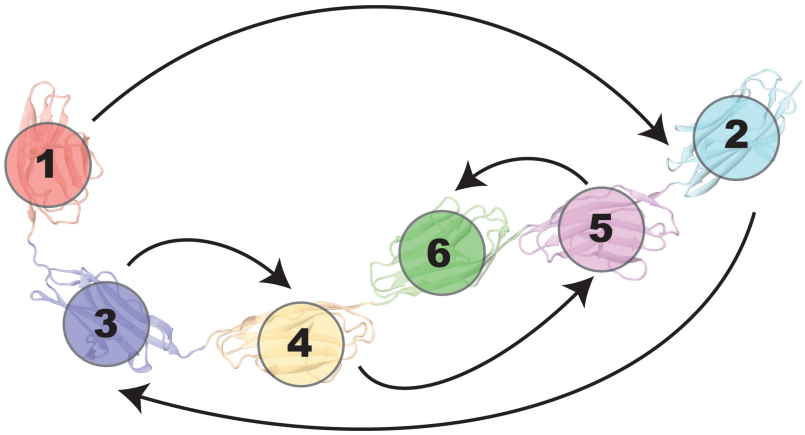

Figure S5: Sequence of domain rupture during stretching of titin Ig65-Ig70 as revealed by simulation *simSTR2*. *simSTR1* and *simSTR2* exhibit the same sequence of rupture events, namely I65 → I70 → I66 → I67 → I69 → I68. Even though cysteines in I65, I66, I67, and I69 are crosslinked by disulfide bonds in *simSTR2*, the rupture sequence is the same as the one seen in the simulation without disulfide bonds (*simSTR1*).

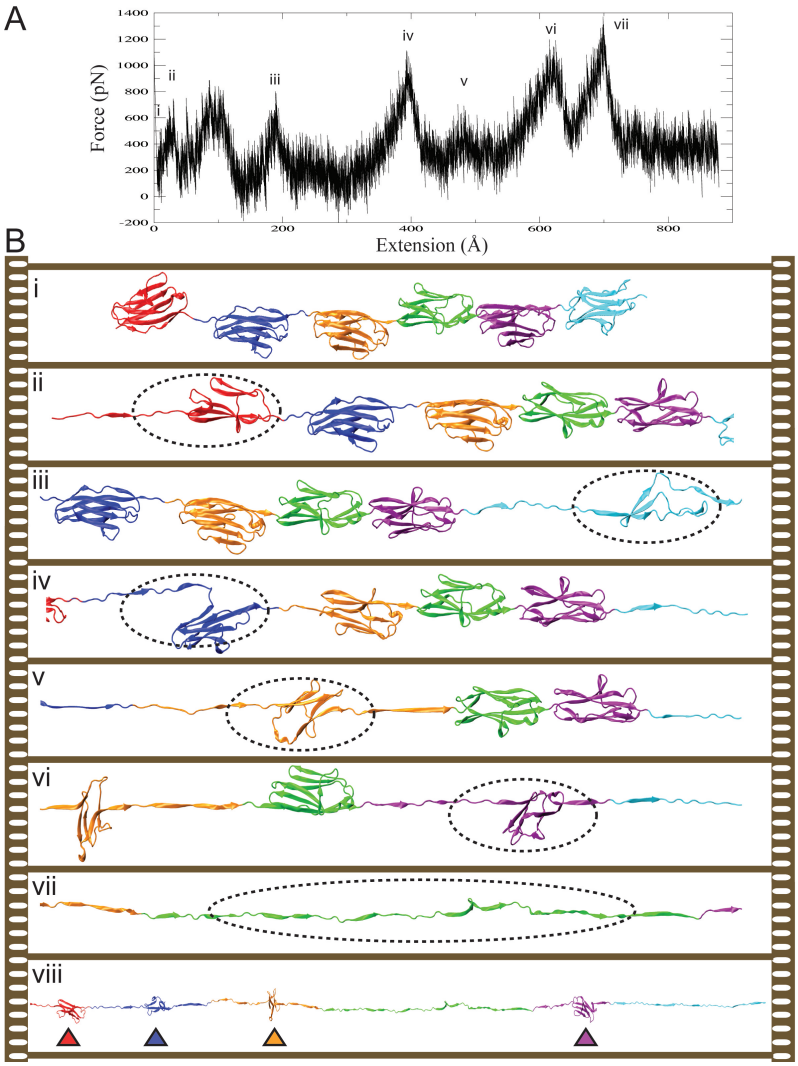

Figure S6: Sequence of domain rupture during stretching of titin I65-I70 in *simSTR2*. For an explanation of A and B as well as the numbering, see Figure 5. *simSTR1* (see Figure 5) and *simSTR2* exhibit the same sequence of rupture events, namely I65 → I70 → I66 → I67 → I69 → I68. Even when cysteines in I65, I66, I67, and I69 were crosslinked with disulfide bonds in *simSTR2*, the rupture sequence did not change from the simulation without disulfide bonds (*simSTR1*).

Simulated refolding of Ig-domain terminal β-strands. It is well known that individual titin domains refold after force is released during force spectroscopy experiments (9; 10). The experimentally observed timescale for refolding a fully extended titin domain, though, is on the order of tens of milliseconds, which is outside of the scope of MD simulations possible

today. Efforts in the past have simulated the refolding of partially unfolded titin I91 (11), beginning from the point where the terminal β-strands (AB and A'G) of I91 have just begun to rupture. Following (11), we performed an MD simulation of a partially unfolded Ig6 structure in order to assess whether refolding could be observed on simulation timescales. The starting configuration for this simulation was taken after extending Ig6 by 60 Å in *simSTR1*. The externally applied force was then set to zero, i.e., Ig6 was then simulated under equilibrium conditions for 18.6 ns. At the beginning of the simulation, two Ig-domains were already partially unfolded, I65 at the N-terminus and I70 at the C-terminus. However, only the N-terminal β-strands of I70 (AB and A'G) had ruptured at this point, whereas I65 had extended more fully, with its A, A', and B β-strands extended from the protein core. Over the course of the simulation, the terminal β-strands of I70 were observed to refold and stabilize their AB and A'G interactions. The extended β-strands of I65, however, did not refold on the relatively short (for refolding) timescale simulated. Snapshots from this simulation are shown in Figure S7, illustrating the refolding of I70 at intervals of 6 ns.

Additional Discussions

Discrepancy between simulated and experimental/biological stretching velocities. SMD simulations describe the mechanical behavior of proteins qualitatively rather well, but magnitude and fluctuations of the monitored forces in constant-velocity SMD simulations depend on stretching velocities and spring constant used (12; 13). Simulations taking months to complete are still far from the timescale (seconds) of experiments. In fact, SMD simulations of Ig domain rupture employ stretching velocities that are orders of magnitude higher than the speeds used in AFM experiments. Therefore, the force peak values seen in simulated force-extension curves are larger than those recorded in experiments. Nonetheless, excellent qualitative agreement between simulation and experiment is found in regard to the force extension relationships (12; 14–20), which reflects the fact that the simulations capture the same rupture mechanism as experiments do as recently demonstrated for the titin domain I91 (7). This domain resembles in its architecture closely domains I65-I70 stretched here. In (7) the authors reduced the speed of Ig91 stretching and rupture to within nearly two orders of magnitude of recent (ms time scale) experiments; the study showed that over a nanosecond-to-second range experimental and simulation data are consistent with the same statistical mechanical model.

It is noteworthy that tertiary structure elasticity is captured much better in simulations than is secondary structure elasticity. For example, in case of ankyrin investigated computationally in (21), the respective tertiary structure elasticity predicted agrees within a factor of 2 with the one measured experimentally later in (22; 23). In the present case, extension

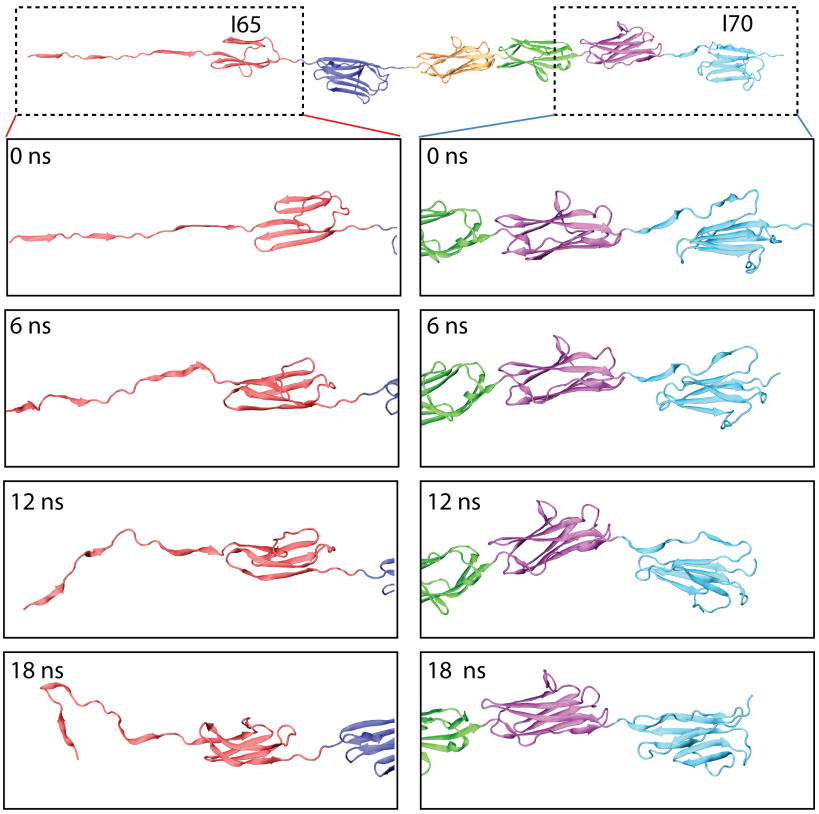

Figure S7: Simulated refolding of Titin I65-70 Ig-domains. After 60 Å extension in *simSTR1*, the force was released and protein allowed to relax. Over 18.6 ns simulation, the partially unfolded I70 domain, whose terminal AB and A'G β-strands had just ruptured, was observed to refold. The more extended I65 domain did not refold during a practical simulation timescale.

of Ig6 up to 100 Å yields a force of 200 pN, a value comparable to the force seen in AFM experiments required to rupture individual Ig domains (9; 24). Assuming an accurate computational description of tertiary structure elasticity (compared to description of secondary structure elasticity), one concludes that Ig6 is stretched by about 100 Å before rupture of its individual domains sets in.

Change in contour length between rupture events. The force extension curve derived from *simSTR1* shows that the contour length increase after domain rupture events is not regularly spaced as expected if domains rupture and unfold completely one-by-one. Analysis of the trajectory shows that the irregular contour length increase is due to domain I65 unfolding in a two-step process: after the terminal AB and A'G β-strands rupture, there is enough compliance in the chain and long I65-I66 linker for the remaining folded segment

of I65 to reorient such that the opposite terminal FG β-strands can resist stretching forces and does not separate. As a result, I65 stops rupturing and, instead, I70 and I66 rupture and fully unfold before I65 completes its rupture. The rupture of the FG strand of some of Ig6's domains can be seen in Figure 5 through force peaks in the force-extension traces for *simSTR1*, for example, the rupture of I70's FG strand between peaks (*iii*) and (*iv*) as well as the rupture of I66 and I65's FG strands between points (*iv*) and (*v*).In our simulations, the two step unfolding of one of Ig6's domains was only observed for the I65 domain in *simSTR1*, since disulfide bonds modeled in *simSTR2* serve to partially constrain the C-terminal β-strand of I65. It is conceivable though, given the similar architecture among Ig-domains in titin, that a two-step unfolding mechanism for the rupture of individual Ig-domains without internal disulfide bonds may also come into play for long flexible Ig-segments in other regions of titin. The correlation of all force peaks in the force extension curve to domain rupture events are illustrated in movies S2 and S3 included in this Supporting Material.

References

1. von Castelmur, E., M. Marino, D. I. Svergun, L. Kreplak, Z. Ucurum-Fotiadis, P. V. Konarev, A. Urzhumtsev, D. Labeit, S. Labeit, and O. Mayans. 2008. A regular pattern of Ig super-motifs defines segmental flexibility as the elastic mechanism of the titin chain. *Proc. Natl. Acad. Sci. USA.* 105:1186–1191.

2. Phillips, J. C., R. Braun, W. Wang, J. Gumbart, E. Tajkhorshid, E. Villa, C. Chipot, R. D. Skeel, L. Kale, and K. Schulten. 2005. Scalable molecular dynamics with NAMD. *J. Comp. Chem.* 26:1781–1802.

3. MacKerell, A. D., Jr., D. Bashford, M. Bellott, R. L. Dunbrack, Jr., J. Evanseck, M. J. Field, S. Fischer, J. Gao, H. Guo, S. Ha, D. Joseph, L. Kuchnir, K. Kuczera, F. T. K. Lau, C. Mattos, S. Michnick, T. Ngo, D. T. Nguyen, B. Prodhom, I. W. E. Reiher, B. Roux, M. Schlenkrich, J. Smith, R. Stote, J. Straub, M. Watanabe, J. Wiorkiewicz-Kuczera, D. Yin, and M. Karplus. 1998. All-atom empirical potential for molecular modeling and dynamics studies of proteins. *J. Phys. Chem. B.* 102:3586–3616.

4. Humphrey, W., A. Dalke, and K. Schulten. 1996. VMD – Visual Molecular Dynamics. *J. Mol. Graphics.* 14:33–38.

5. Grubmüller, H., H. Heller, A. Windemuth, and K. Schulten. 1991. Generalized Verlet algorithm for efficient molecular dynamics simulations with long-range interactions. *Mol. Sim.* 6:121–142.

6. Schlick, T., R. Skeel, A. Brünger, L. Kalé, J. A. Board Jr., J. Hermans, and K. Schulten. 1999. Algorithmic challenges in computational molecular biophysics. *J. Comp. Phys.* 151:9–48.

7. Lee, E. H., J. Hsin, M. Sotomayor, G. Comellas, and K. Schulten. 2009. Discovery through the computational microscope. *Structure.* 17:1295–1306.

8. Mayans, O., J. Wuerges, S. Canela, M. Gautel, and M. Wilmanns. 2001. Structural evidence for a possible role of reversible disulphide bridge formation in the elasticity of the muscle protein titin. *Structure.* 9:331–340.

9. Rief, M., M. Gautel, F. Oesterhelt, J. M. Fernandez, and H. E. Gaub. 1997. Reversible unfolding of individual titin immunoglobulin domains by AFM. *Science.* 276:1109–1112.

10. Minajeva, A., M. Kulke, J. M. Fernandez, and W. A. Linke. 2001. Unfolding of titin domains explains the viscoelastic behavior of skeletal myofibrils. *Biophys. J.* 80:1442–1451.

11. Gao, M., H. Lu, and K. Schulten. 2001. Simulated refolding of stretched titin immunoglobulin domains. *Biophys. J.* 81:2268–2277.

12. Izrailev, S., S. Stepaniants, M. Balsera, Y. Oono, and K. Schulten. 1997. Molecular dynamics study of unbinding of the avidin-biotin complex. *Biophys. J.* 72:1568–1581.

13. Evans, E. and K. Ritchie. 1997. Dynamic strength of molecular adhesion bonds. *Biophys. J.* 72:1541–1555.

14. Gao, M., D. Craig, O. Lequin, I. D. Campbell, V. Vogel, and K. Schulten. 2003. Structure and functional significance of mechanically unfolded fibronectin type III1 intermediates. *Proc. Natl. Acad. Sci. USA*. 100:14784–14789.

15. Isralewitz, B., M. Gao, and K. Schulten. 2001. Steered molecular dynamics and mechanical functions of proteins. *Curr. Opin. Struct. Biol.* 11:224–230.

16. Lu, H., B. Isralewitz, A. Krammer, V. Vogel, and K. Schulten. 1998. Unfolding of titin immunoglobulin domains by steered molecular dynamics simulation. *Biophys. J.* 75:662–671.

17. Marszalek, P. E., H. Lu, H. Li, M. Carrion-Vazquez, A. F. Oberhauser, K. Schulten, and J. M. Fernandez. 1999. Mechanical unfolding intermediates in titin modules. *Nature*. 402:100–103.

18. Ortiz, V., S. O. Nielsen, M. L. Klein, and D. E. Discher. 2005. Unfolding a linker between helical repeats. *J. Mol. Biol.* 349:638–647.

19. Rief, M. and H. Grubmüller. 2002. Force spectroscopy of single biomolecules. *CHEMPHYSCHEM*. 3:255–261.

20. Sotomayor, M., V. Vasquez, E. Perozo, and K. Schulten. 2007. Ion conduction through MscS as determined by electrophysiology and simulation. *Biophys. J.* 92:886–902.

21. Sotomayor, M., D. P. Corey, and K. Schulten. 2005. In search of the hair-cell gating spring: Elastic properties of ankyrin and cadherin repeats. *Structure*. 13:669–682.

22. Lee, G., K. Abdi, Y. Jiang, P. Michaely, V. Bennett, and P. E. Marszalek. 2006. Nanospring behaviour of ankyrin repeats. *Nature*. 440:246–249.

23. Li, L., S. Wetzel, A. Plückthun, and J. M. Fernandez. 2006. Stepwise unfolding of ankyrin repeats in a single protein revealed by atomic force microscopy. *Biophys. J.* 90:L30–L32.

24. Carrion-Vazquez, M., A. Oberhauser, S. Fowler, P. Marszalek, S. Broedel, J. Clarke, and J. Fernandez. 1999. Mechanical and chemical unfolding of a single protein: A comparison. *Proc. Natl. Acad. Sci. USA*. 96:3694–3699.